LIGHT CAPTURE AND PIGMENT DIVERSITY IN MARINE AND FRESHWATER CRYPTOPHYTES[1]

Brady R. Cunningham

School of the Earth, Ocean & Environment, University of South Carolina, Columbia, South Carolina 29208, USA

Matthew J. Greenwold

Department of Biological Sciences, University of South Carolina, Columbia, South Carolina 29208, USA

Eric M. Lachenmyer, Kristin M. Heidenreich, Abigail C. Davis

School of the Earth, Ocean & Environment, University of South Carolina, Columbia, South Carolina 29208, USA

Jeffry L. Dudycha

Department of Biological Sciences, University of South Carolina, Columbia, South Carolina 29208, USA

and Tammi L. Richardson[2] iD

School of the Earth, Ocean & Environment, University of South Carolina, Columbia, South Carolina 29208, USA
Department of Biological Sciences, University of South Carolina, Columbia, South Carolina 29208, USA

Phenotypic traits associated with light capture and phylogenetic relationships were characterized in 34 strains of diversely pigmented marine and freshwater cryptophytes. Nuclear SSU and partial LSU rDNA sequence data from 33 of these strains plus an additional 66 strains produced a concatenated rooted maximum likelihood tree that classified the strains into 7 distinct clades. Molecular and phenotypic data together support: (i) the reclassification of *Cryptomonas irregularis* NIES 698 to the genus *Rhodomonas*, (ii) revision of phycobiliprotein (PBP) diversity within the genus *Hemiselmis* to include cryptophyte phycocyanin (Cr-PC) 569, (iii) the inclusion of previously unidentified strain CCMP 2293 into the genus *Falcomonas*, even though it contains cryptophyte phycoerythrin 545 (Cr-PE 545), and (iv) the inclusion of previously unidentified strain CCMP 3175, which contains Cr-PE 545, in a clade with PC-containing *Chroomonas* species. A discriminant analysis-based model of group membership correctly predicted 70.6% of the clades using three traits: PBP concentration $\cdot$ cell^{-1}, the wavelength of PBP maximal absorption, and habitat. Non-PBP pigments (alloxanthin, chl-*a*, chl-*c₂*, α-carotene) did not contribute significantly to group classification, indicating the potential plasticity of these pigments and the evolutionary conservation of the PBPs. Pigment data showed evidence of trade-offs in investments in PBPs vs. chlorophylls ($a + c_2$).

Key index words: absorption; LSU rDNA; phycobilins; phycobiliproteins; phylogeny; pigments; PUR; spectral irradiance

Abbreviations: CTAB, cetyltrimethyl ammonium bromide; PBP, phycobiliprotein

Cryptophytes are a widespread yet poorly characterized group of unicellular eukaryotic algae that inhabit ponds, lakes, estuaries, and oceans (Klaveness 1988, Hoef-Emden 2008, Hoef-Emden and Archibald 2016). Cryptophytes originated via secondary endosymbiosis (engulfment of a red algal cell by an unknown eukaryote), which led to the evolution of pigments that are unique among algae (Archibald and Keeling 2002, Bhattacharya et al. 2004, Gould et al. 2008). Cryptophytes are thus complex with respect to their genetic and cellular structure, and are distinctive in their pigmentation and the organization of these pigments within the plastids (Gould et al. 2007).

Visually, cryptophytes vary markedly in color (Fig. S1 in the Supporting Information). These variations arise from differences in the type of phycobiliprotein (PBP) produced by the cell. Cryptophyte strains contain a single type of phycoerythrin or phycocyanin, but not both (Hill and Rowan 1989). Eight types of cryptophyte PBPs have been defined: three cryptophyte phycoerythrins (Cr-PE) (Cr-PE 545, Cr-PE 555, and Cr-PE 566) and five cryptophyte phycocyanins (Cr-PC) (Cr-PC 569, Cr-PC 577, Cr-PC 615, Cr-PC 630, and Cr-PC 645), all of which are

named according to the approximate wavelength of maximum absorption of the PBP (Hill and Rowan 1989, Hoef-Emden and Archibald 2016). In part, taxonomic classification to genus level is related to the type of PBP. For example, all known *Rhodomonas* species contain Cr-PE 545. However, PBP type cannot be used solely to classify cryptophytes to genus (Hill and Rowan 1989). Strains containing Cr-PE 545, for example, may belong to one of several genera including *Rhodomonas, Geminigera, Guillardia,* or *Proteomonas* (Hoef-Emden 2008, Hoef-Emden and Archibald 2016). Researchers now usually combine information on strain-specific PBP type with cellular ultrastructure and molecular data to classify cryptophytes to genus and species (Hill and Rowan 1989, Hoef-Emden and Melkonian 2003, Hoef-Emden 2008, Hoef-Emden and Archibald 2016).

We measured phenotypic traits related to light absorption (PBP type, PBP concentrations, non-PBP pigment concentrations, whole cell absorption spectra, photosynthetically usable radiation (PUR), and cell volume) for 34 strains of cryptophytes. These traits allowed us to assess aspects of phenotypic diversity related to light capture. We constructed molecular phylogenies using SSU and LSU rDNA data from 33 of our strains and sequences downloaded from the National Center for Biotechnology Information (NCBI) for 66 others. Then, recognizing that light absorption likely has genetic roots, we used discriminant analysis to determine which phenotypic traits best predicted clade membership. Our results illustrate the remarkable genetic and phenotypic diversity even within this subset of cryptophytes, and provide new information about links between phylogenetic and functional diversification in this group of microalgae.

METHODS

Cryptophyte cultures. Cryptophyte strains were acquired from six culture repositories (details in Table S1 in the Supporting Information). All were grown in batch culture on a 12:12 h light:dark cycle at 30 μmol photons · m^{-2} · s^{-1} with illumination provided from the side by Daylight Deluxe Arctic White 32-watt fluorescent lamps (Philips, Inc. NJ). All cultures were grown in 250 mL Pyrex® flasks with no more than 150 mL of culture in each and were gently swirled by hand each day. Growth temperatures and culture media were as described in Table S1. All stock cultures were transferred to fresh culture media while in the exponential phase. Samples for phenotypic characterization were taken in triplicate from a single culture in mid-exponential phase as determined by cell counts. Means and standard deviations, therefore, represent analytical variability, i.e., are technical replicates, but do not represent any possible within-strain variability under the same culture conditions.

Light absorption. Absorbance spectra for each cryptophyte strain were acquired with a Shimadzu dual-beam UV/VIS 2450 spectrophotometer, using the filter pad technique (Shibata 1958, Roesler 1998). For each replicate, 5–10 mL of sample was filtered onto a Whatman GF/F filter (GE Life Sciences, Buckinghamshire, UK). A blank GF/F, through which only culture medium was filtered, served as reference. All samples were stored at −80°C until analysis. Samples were

scanned from 400 to 800 nm at 1 nm intervals. Spectra were scatter-corrected by subtracting the average absorbance between 730 and 750 nm from the spectrum (Shibata 1958). Scattering was minimized by ensuring that each filter was fully loaded with material (Roesler 1998). Log$_{10}$ absorbance values were then converted to chl-*a* -specific absorption coefficients (a^{Chl}) according to:

$$a^{\text{Chl}}(\lambda) = \frac{2.303 \cdot A(\lambda)}{L \cdot \beta \cdot N}, \tag{1}$$

where $A(\lambda)$ = the wavelength-dependent absorbance, L = the optical path length of the particles on the filter (i.e., sample volume divided by clearance area of the filter), N = the concentration of chl-*a* in the culture, and β = the path length amplification factor. Because the filters had a high particle load, a β correction factor of 2.0 was used (Roesler 1998).

Photosynthetically usable radiation. Photosynthetically usable radiation (in μmol photons · m^{-2} · s^{-1}) was calculated for each cryptophyte strain as:

$$\text{PUR} = \int_{400}^{200} \text{PAR}(\lambda)\bar{A}(\lambda)d\lambda, \tag{2}$$

where the weighting function $\bar{A}(\lambda)$ represents the probability that a photon with a given wavelength is absorbed by the cell (Morel 1978). It is derived from the absorption spectrum $a^{\text{Chl}}(\lambda)$, measured as described above, normalized to its maximum absorption ($a^{\text{Chl}}_{\text{max}}$) in the full spectrum light environment of the culture incubators. A flame spectrometer (Ocean Optics, Dunedin, FL, USA) was used to measure the spectral distribution of available irradiance in the incubators (400–700 nm at 1 nm intervals) just outside of culture containers.

PBP analysis by spectroscopy. Cryptophyte PBP concentrations were determined using the freeze/thaw centrifugation method of Lawrenz et al. (2011). Aliquots (40–50 mL) of mid-exponential phase culture of each strain were sampled and then centrifuged at 2,054*g* for 10 min. The resulting supernatant was decanted and the pellet re-suspended in 0.1 M phosphate buffer (pH = 6) and homogenized using a vortexer. Samples were then placed at −20°C for 2 h until frozen. Once frozen, samples were moved to 5°C to thaw for 24 h. Thawed samples were centrifuged at 10,870*g* for 5 min to remove excess cellular debris. The absorbance of each sample extract was measured from 400 to 750 nm at 1-nm intervals with a Shimadzu UV-VIS 2450 dual beam spectrophotometer using a 1-cm quartz glass cuvette against a phosphate buffer blank. Data were scatter-corrected by subtracting absorbance at 750 nm from the maximum PBP absorption peak (Lawrenz et al. 2011). PBP concentration (c; pg · cell^{-1}) was calculated according to:

$$c = \frac{A}{\varepsilon \cdot d} \times \text{MW} \times \frac{V_{\text{buffer}}}{V_{\text{sample}}} \times \frac{10^{12}}{N} \tag{3}$$

where A = absorbance of sample, ε = the extinction coefficient for Cr-PE (5.67×10^5 L · mol^{-1} · cm^{-1}; MacColl et al. 1976) or Cr-PC (5.7×10^5 L · mol^{-1} · cm^{-1}; MacColl et al. 1973) d = path length of the cuvette in cm, MW = molecular weight of Cr-PE = 45,000 Da or Cr-PC = 50,000 Da, V_{buffer} and V_{sample} = volume of buffer and sample, respectively, N is the concentration of cells (cells · L^{-1}), and 10^{12} is a conversion factor to convert the result to pg · cell^{-1}. Molecular weights were averages of values presented in MacColl et al. (1973, 1976), Gantt (1979), and Overkamp et al. (2014a,b) for Cr-PE or Cr-PC containing cryptophytes.

HPLC pigment analysis. Non-PBP pigments (chl-*a*, chl-*c$_2$*, alloxanthin, and α-carotene) were analyzed by HPLC according to Pinckney et al. (1996). Samples from each

cryptophyte culture were lyophilized for 24 h at −50°C, placed in 1.5 mL 90% acetone and extracted at −20°C for 24 h. Filtered extracts (350 μL) were injected into a Shimadzu liquid chromatograph with photodiode array detector. Pigment peaks were identified and quantified by comparison of retention times and absorption spectra with pure standards (DHI, Denmark Hørsholm). The synthetic carotenoid β-apo-8′-carotenal (Sigma) was used as an internal standard. Full details of protocols for extraction, instrumentation and analysis, calibration, validation, and data products can be found at: https://www.researchgate.net/profile/James_Pinckney/publication/265999187_The_USC_HPLC_Method_-Technical_Description/links/55266d0d0cf2628d5afdf397/The-USC-HPLC-Method-Technical-Description.pdf.

Cell size, cell volume, and cell counts. Cell size was determined via light microscopy using a Nikon Eclipse TS100 inverted microscope on at least 200 cells of each strain. Two dimensions, height (h) and diameter (d), were measured on live, but nonswimming, cells using an automated program (Infinity Analyze V6.5; Lumenera Corporation, Nepean, ON, Canada). Volumes (V) were calculated assuming each cell was a prolate spheroid with $V = \pi/6 * h * d^2$ (Hillebrand et al. 1999). Cell counts were done using a Guava EasyCyte HPL Benchtop Flow Cytometer (EMD Millipore). Because cell counts were less time-consuming than measuring cell volumes, at least 400 cells of each strain were counted to give an accuracy of ±10% of the count (Lund et al. 1958, Guillard and Sieracki 2005).

DNA extraction, PCR, and sequencing. Approximately, 2 L of each cryptophyte culture were spun down in a Beckman J2-21 centrifuge using a JA-10 rotor at 7,000 (8,651g) for 30 min. The resulting cell pellet was resuspended in a 2 mL microcentrifuge tube and centrifuged for 12–15 min at 1200–3600g in a Beckman-Coulter Microfuge-18 centrifuge. DNA extraction was conducted using a standard cetyltrimethyl ammonium bromide (CTAB) method. The cell pellet was resuspended in CTAB buffer and lysed overnight at ~56°C, then re-pelleted. The supernatant was extracted and subjected to an RNaseA treatment for 15 min. Two phenol:chloroform:isoamyl alcohol (25:24:1) extractions were then performed, followed by two chloroform:isoamyl alcohol (24:1) extractions. Two volumes of 100% ethanol were then added and the DNA was allowed to precipitate overnight in a −20°C freezer. The resulting DNA pellet was washed with 70% ethanol and dried in a 37°C drying oven. The DNA pellet was then re-suspended in 100 μL of TE buffer (pH 8.0).

Following Marin et al. (1998) and Hoef-Emden (2008) we amplified the nuclear SSU and LSU rDNA using a primary PCR followed by a secondary gene specific (SSU or LSU rDNA) PCR reaction. Unlike Marin et al. (1998) and Hoef-Emden (2008), we did not use biotinylated fluorescent primers for sequencing on an Li-Cor DNA Sequencer; instead, we used standard primers and Applied Biosystems 3730xl DNA analyzer. Our primary PCR reaction was conducted using the nuclear SSU_CrN1F primer and nuclear LSU_1433R primers developed by Marin et al. (1998) using Hoef-Emden (2008) PCR reaction conditions (95°C, 4 min; 30 cycles [95°C, 1 min; 60°C, 2 min; 68°C, 6 min]). Due to read length quality limits of our sequencing platform (~700 bps), we developed three sets of overlapping primers to amplify ~1,600 bps of the nuclear SSU rDNA sequence and two sets of overlapping primers to amplify the 900+ bps of the "partial" LSU rDNA sequence (see Table S2 in the Supporting Information for secondary primer sequences and reaction details). The resulting PCR products were sent to Functional Biosciences (Madison, WI, USA) for forward- and reverse-read sequencing. We processed reads using SeqTrace (Stucky 2012) and EMBOSS merger (http://www.bioinforma

tics.nl/cgi-bin/emboss/help/merger) to verify base calls and to assemble sequences for analysis (Rice et al. 2000).

Phylogeny reconstruction. We sequenced the nuclear SSU and partial LSU rDNA of 33 strains and combined this information with SSU and LSU sequences of 66 additional strains downloaded from National Center for Biotechnology Information (NCBI; Table S3 in the Supporting Information).

The SSU and LSU nucleotide sequences of the 99 strains were aligned separately with ClustalW2 (Larkin et al. 2007) and then concatenated. The concatenated alignment was visually inspected and edited using the BioEdit Sequence Alignment Editor (Hall 1999). PartitionFinder2 (Lanfear et al. 2016) was used to determine the best-fitting nucleotide substitution model and confirmed that the best partitioning scheme was the original separation of the SSU and LSU sequences. The data partitions for SSU and LSU were 2,086 and 1,681 characters, respectively. Both partitions' best substitution model was a general time reversal model with a portion of invariant sites and a gamma distribution (GTR+I+G), which was then used for phylogenetic estimation.

We estimated phylogeny with maximum likelihood (ML) and Bayesian approaches. For the ML analysis, RAxML v8.2.7 (Stamatakis 2014) was run using the autoMRE option that automatically stops performing bootstrap replicates once convergence has been reached (Pattengale et al. 2009). For this data set, convergence was reached after 250 replicates. The resulting bootstrap replicates were then mapped onto the phylogeny with the best likelihood score out of 1,000 thorough ML searches. For the Bayesian phylogeny, we used MrBayes v3.2 (Ronquist et al. 2012). The concatenated alignment was run in duplicate with 4 chains and 10,000,000 generations, which produced an average standard deviation of split frequencies of 0.0088. Convergence was evaluated using the potential scale reduction factor (PSRF; Gelman and Rubin 1992) and plots of the generation versus the log-probability of observing the data. Following phylogenetic estimation, *Goniomonas* sp. ATCC 50108 and *Goniomonas truncata* TMG005 were used as outgroups based on other cryptophyte phylogenies (Hoef-Emden 2008, Hoef-Emden and Archibald 2016).

Statistics. Relationships between cryptophyte phenotypic characteristics and molecular phylogenetic clade classification were determined using stepwise discriminant analysis with the grouping variable as clade classification, set between 1 and 7 (SPSS V24; IBM Armonk, NY, USA). This analysis was used to build a predictive model of cryptophyte clade membership based on the observed phenotypic characteristics for each strain: cell volume, PUR, wavelength of maximum PBP absorption, cellular concentrations of PBP, chl-a, chl-c_2, alloxanthin, and α-carotene, and cell volume concentrations of PBP, chl-a, chl-c_2, alloxanthin, and α-carotene.

RESULTS

The strains investigated include examples of all known variations of PBPs that have been associated with cryptophytes (Glazer and Wedemayer 1995). Whole cell absorption spectra for representative strains of each Cr-PBP type (Fig. S2 in the Supporting Information) show the multiple peaks that represent the bulk absorption properties of all of the photopigments (Tables 1 and 2) that produce the variations in color observed among strains (Fig. S1).

Among our strains, cell volumes varied 75-fold, ranging from 23 ± 9 μm^3 for *Hemiselmis tepida* CCMP 443 to $1,718 \pm 520$ μm^3 for *Cryptomonas*

tetrapyrenoidosa CCAP 979/26 (now called *Cryptomonas curvata*, see details in Table 1). Calculated PUR varied by less than threefold, ranging from 4.7 µmol quanta $\cdot$ m^{-2} $\cdot$ s^{-1} for *Hemiselmis cryptochromatica* CCMP 1181 to 12.2 µmol quanta $\cdot$ m^{-2} $\cdot$ s^{-1} for *Chroomonas* sp. SCCAP K1623 (Table 1). *Rhodomonas falcata* NIES 702 had the lowest relative concentration of PBP (<10% of total cell pigment), while *Chroomonas* sp. CCMP 270 had the highest (>90% of total cell pigment; Fig. 1). Chlorophyll *a* and *c₂* concentrations varied by more than two orders of magnitude, largely in tandem with each other (Table 2; Fig. 1). Alloxanthin and α-carotene were generally minor components of the total pigment complement (Table 2; Fig. 1).

Our phylogeny grouped the 99 strains into 7 distinct clades and 1 phylogenetically isolated strain (Fig. 2, see also Fig. S3 in the Supporting Information). Clade 1 included strains mainly from the genera *Chroomonas* and *Hemiselmis*. Clade 2 included all *Cryptomonas* strains except *C. irregularis* and *C. acuta*. Clade 3 comprised two strains, the unidentified strains CCMP 2293 and *Falcomonas daucoides* ShP-CSU, while Clade 4 had Hanusia *phi* CCMP 325 and *Guillardia theta* CCMP 327. Clade 5 comprised strains of *Rhodomonas*, *Storeatula* sp. CCMP 1868, and *Cryptomonas irregularis* NIES 698. Clade 6 had *Rhodomonas minuta* CPCC344 and *Geminigera cryophila* CCMP 2564, while Clade 7 consisted of *Proteomonas sulcata* CCMP 1175, *Proteomonas* sp. CCMP 2715, and *Cryptomonas acuta* NIES 697. The single isolated strain was the unidentified strain CCMP 1179.

Clades varied with respect to their diversity of PBP pigment type. Clade 1, for example, included *Hemiselmis* strains that contain Cr-PE 555, Cr-PC 569, Cr-PC 577, or Cr-PC 615 and *Chroomonas* with Cr-PC 630 and Cr-PC 645 (Fig. 1). Clade 2, in contrast, comprised exclusively freshwater *Cryptomonas* strains with Cr-PE 566. Clades 3 to 7 contained freshwater or marine strains with Cr-PE 545, including *C. irregularis* strain in Clade 5 and *C. acuta* in Clade 7.

A typical absorption spectrum for Clade 2 *Cryptomonas* strains is represented by the *C. pyrenoidifera* CCMP 1167 spectrum (Fig. 3A). A typical absorption spectrum for Clade 5 is that of *Rhodomonas salina* CCMP 1319 (Fig. 3C). The shape of the absorption spectrum for *C. irregularis* NIES 698 (Clade 5; Fig. 3B), matches that of *R. salina* much more closely than that of its fellow *Cryptomonas* strains (see also Fig. S2C for *C. ovata* UTEX 2783). *Cryptomonas acuta* (Clade 7) also contains Cr-PE 545 and has an absorption spectrum very similar to that of *C. irregularis* (Fig. S4A in the Supporting Information). The monophyletic strain, unidentified CCMP 1179, contains Cr-PE 545 and is our sole estuarine strain.

Three phenotypic traits (wavelength of maximum PBP absorption, PBP per cell and habitat) together accounted for 77.8% of the variance in our constructed phylogenetic tree (Table S4 in the Supporting Information). Three discriminant functions were identified and weightings resulted in a model that correctly classified 70.6% of the original grouped cases (Wilks' Lambda =0.051, χ^2 = 81.773, df = 21, P = 0.000; Table S4).

DISCUSSION

We have presented a broad comparison of key traits involved in light capture within the Cryptophyta, a phylum that is unique among the eukaryotes in its remarkable diversity of pigmentation, resulting in wide variations in spectral absorption capabilities even between closely related strains. Values for our phenotypic measurements fell well within the bounds of those in the literature. Hoef-Emden and Archibald (2016) and Hoef-Emden (2018) report a size range of 5–50 µm for cryptophytes in general, which encompasses the sizes all of the strains we measured. Cellular pigment content was available from the literature for a few strains. Cr–PE concentrations for *Pyremonas* (now *Rhodomonas*) *salina* (strain C3, a synonym for our strain CCMP 1319) as reported by Lewitus and Caron (1990) were ~5 pg $\cdot$ cell^{-1}, while chl-*a* for the same strain was reported as 0.7–0.8 pg $\cdot$ cell^{-1}. These concentrations are lower than ours (11.1 pg $\cdot$ cell^{-1} for PE, 1.7 pg $\cdot$ cell^{-1} for chl-*a*), but culture conditions differed and cell size was not reported so it is difficult to compare directly but the ratios of PE: chl-*a* between their study and ours (~6.3–7.1 g:g vs. 6.5 g:g, respectively) agree very well. Nicklisch and Steinberg (2009) report cellular chl-*a* concentrations from 0.3 to 0.5 pg $\cdot$ cell^{-1} (depending on light exposure and nutrient status) for *R. minuta* (strain unknown), which is lower than our value of 1.1 pg $\cdot$ cell^{-1} for strain CPCC 344. Vesk and Jeffrey (1977) reported a PE:chl-*a* ratio for *Chroomonas* sp. (Port Hacking isolate) of 4.8 and 6.3 g:g for cultures grown under white and blue-green light respectively. Otherwise, there is a general paucity of data on pigment concentrations and light absorption characteristics in the literature, either for whole cells or for extracted PBP pigments. As exceptions, Kamiya and Miyachi (1984) show an absorption spectrum for Cr-PE 545 that mirrors ours for the same strains (*H. phi*), and Hoef-Emden (2008) presents absorption spectra for several types of cryptophyte PBPs. Her spectrum for Cr-PC 645 for *Chroomonas* sp. CCMP 1221 matches ours (Fig. S5 in the Supporting Information), as do her spectra for Cr-PE 555 from *Hemiselmis rufescens* CCMP 440 (Fig. S6 in the Supporting Information) and PC-577 from *Hemiselmis pacifica* CCMP 706 (Fig. S6). We could find no published spectra for PBPs extracted from the other strains in our study.

Comparison to published phylogenies. The clades within our phylogenetic tree are partially congruent with the taxonomic associations in previously

TABLE 1. Cryptophyte strains used in this study, their habitat, cell volumes, PUR values, and phycobiliprotein (PBP) concentrations. Strain source abbreviations: Culture Collection of Algae and Protozoa (CCAP); National Center for Marine Algae and Microbiota (NCMA, formerly CCMP); The Culture Collection of Algae at the University of Texas at Austin (UTEX); Microbial Culture Collection at the National Institute for Environmental Studies (NIES); Canadian Phycological Culture Center (CPCC); Scandinavian Culture Collection of Algae and Protozoa (SCCAP).

Strain	Clade	Habitat	PBP peak absorption (nm)	PUR (μmol photons $\cdot$ m^{-2} $\cdot$ s^{-1})	PBP conc (pg$\cdot$cell^{-1})	Cell volume (μm^3)	PBP conc (pg $\cdot$ μm^{-3})
Chroomonas mesostigmatica CCMP 1168	1	Marine	645	6.0	2.3 ± 0.2	134 ± 40	0.02
Chroomonas norstedtii NIES 708	1	Fresh	630	9.4	6.5 ± 1.0	203 ± 57	0.03
Chroomonas sp. CCMP 1221	1	Marine	645	8.7	4.6 ± 0.7	106 ± 30	0.04
Chroomonas sp. CCMP 270	1	Marine	645	11.7	15.3 ± 1.2	108 ± 41	0.14
Chroomonas sp. SCCAP K1623	1	Fresh	630	12.2	10.7 ± 0.3	369 ± 117	0.03
Cryptomonas acuta NIES 697	7	Marine	545	6.3	6.2 ± 0.4	357 ± 89	0.02
Cryptomonas irregularis NIES 698	5	Marine	545	5.8	8.4 ± 1.2	887 ± 274	0.01
Cryptomonas lucens CCAP 979/35	2	Fresh	566	8.7	29.3 ± 4.9	1,290 ± 453	0.02
Cryptomonas ovata UTEX 2783	2	Fresh	566	8.4	25.7 ± 5.1	1,079 ± 290	0.02
Cryptomonas pyrenoidifera CCMP 1167	2	Fresh	566	5.6	40.4 ± 10.7	708 ± 219	0.06
Cryptomonas sp. CPCC 336	2	Fresh	566	9.0	16.4 ± 8.4	323 ± 83	0.05
Cryptomonas curvata CCAP 979/26*	2	Fresh	566	8.4	16.5 ± 2.1	1,718 ± 520	0.01
Geminigera cryophila CCMP 2564	6	Marine	545	5.6	6.6 ± 1.9	1,076 ± 389	0.01
Guillardia theta CCMP 327	4	Marine	545	5.4	0.9 ± 0.1	139 ± 42	0.01
Hanusia phi CCMP 325	4	Marine	545	5.0	1.9 ± 0.2	199 ± 55	0.01
Hemiselmis andersenii CCMP 644	1	Marine	555	5.9	1.6 ± 0.1	54 ± 19	0.03
Hemiselmis cryptochromatica CCMP 1181	1	Marine	569	4.7	0.2 ± 0.0	30 ± 12	0.01
Hemiselmis pacifica CCMP 706	1	Marine	577	8.8	1.3 ± 0.1	91 ± 44	0.01
Hemiselmis rufescens CCMP 440	1	Marine	555	5.2	1.1 ± 0.0	31 ± 13	0.04
Hemiselmis tepida CCMP 443	1	Marine	615	7.1	0.5 ± 0.2	23 ± 9	0.02
Proteomonas sp. CCMP 2715	7	Marine	545	6.3	1.2 ± 0.1	98 ± 28	0.01
Proteomonas sulcata CCMP 1175	7	Marine	545	6.5	10.3 ± 2.3	279 ± 118	0.04
Rhinomonas reticulata CCAP 995/2	5	Marine	545	6.9	3.3 ± 1.0	187 ± 64	0.02
Rhodomonas abbreviata CCMP 1178	5	Marine	545	5.7	3.8 ± 1.5	543 ± 172	0.01
Rhodomonas atrorosea CCAP 978/6A	5	Marine	545	5.6	4.4 ± 0.6	230 ± 65	0.02
Rhodomonas chrysoidea NIES 701	5	Marine	545	6.2	11.9 ± 3.6	266 ± 88	0.04
Rhodomonas falcata NIES 702	5	Marine	545	7.1	2.6 ± 0.4	417 ± 152	0.01
Rhodomonas lens CCMP 739	5	Marine	545	6.1	13.9 ± 4.4	284 ± 91	0.05
Rhodomonas minuta CPCC 344	6	Fresh	545	6.0	4.3 ± 0.7	111 ± 38	0.04
Rhodomonas salina CCMP 1319	5	Marine	545	6.7	11.1 ± 1.2	213 ± 61	0.05
Storeatula sp. CCMP 1868	5	Marine	545	6.3	14.6 ± 0.8	569 ± 172	0.03
Unidentified sp. CCMP 1179	–	Estuary	545	6.7	2.1 ± 0.3	249 ± 75	0.01
Unidentified sp. CCMP 2293	3	Marine	545	6.2	2.3 ± 0.1	95 ± 24	0.02
Unidentified sp. CCMP 3175	1	Marine	545	6.6	3.9 ± 0.6	131 ± 37	0.03

*Note that CCAP 979/26 was supplied to us as *Cryptomonas tetrapyrenoidosa* but that the name of this strain has been changed to *Cryptomonas curvata* (Hoef-Emden and Melkonian 2008). Unidentified sp. CCMP 1179 did not fall into any of the 7 clades (–). Errors are standard deviations of triplicate measurements.

TABLE 2. HPLC-derived pigment concentrations for cryptophyte strains in this study. Source abbreviations: Culture Collection of Algae and Protozoa (CCAP); National Center for Marine Algae and Microbiota (NCMA, formerly CCMP); The Culture Collection of Algae at the University of Texas at Austin (UTEX); Microbial Culture Collection at the National Institute for Environmental Studies (NIES); Canadian Phycological Culture Center (CPCC); Scandinavian Culture Collection of Algae and Protozoa (SCCAP).

Strain	chl-a (pg·cell^{-1})	chl-c_2 (pg·cell^{-1})	Allox (pg·cell^{-1})	α-carotene (pg·cell^{-1})	chl-a (pg · μm^{-3})	chl-c_2 (pg · μm^{-3})	Allox (pg · μm^{-3})	α-carotene (pg · μm^{-3})
Chroomonas mesostigmatica CCMP 1168	0.4 ± 0.0	0.5 ± 0.0	0.2 ± 0.0	0.2 ± 0.0	0.003	0.004	0.002	0.001
Chroomonas norstedtii NIES 708	3.1 ± 0.5	1.2 ± 0.4	0.9 ± 0.2	0.9 ± 0.3	0.015	0.006	0.004	0.004
Chroomonas sp. CCMP 1221	0.3 ± 0.1	0.6 ± 0.2	0.2 ± 0.0	0.1 ± 0.0	0.003	0.006	0.002	0.001
Chroomonas sp. CCMP 270	3.4 ± 0.1	3.5 ± 0.0	9.8 ± 0.0	6.2 ± 0.0	0.007	0.002	0.002	0.005
Chroomonas sp. SCAAP K1623	1.6 ± 0.2	0.7 ± 0.2	0.6 ± 0.1	0.4 ± 0.1	0.004	0.002	0.002	0.001
Cryptomonas acuta NIES 697	24.7 ± 1.3	40.2 ± 4.3	7.0 ± 0.5	6.9 ± 1.1	0.069	0.113	0.020	0.019
Cryptomonas irregularis NIES 698	22.6 ± 0.3	37.7 ± 5.3	6.4 ± 0.1	5.9 ± 0.2	0.025	0.043	0.007	0.007
Cryptomonas lucens CCAP 979/35	5.3 ± 0.3	4.3 ± 0.9	1.2 ± 0.1	1.0 ± 0.1	0.004	0.003	0.001	0.001
Cryptomonas ovata UTEX 2783	9.5 ± 0.6	7.5 ± 0.4	2.8 ± 0.9	2.7 ± 0.2	0.009	0.007	0.003	0.003
Cryptomonas pyrenoidifera CCMP 1167	4.5 ± 0.1	5.5 ± 0.3	2.2 ± 0.1	0.8 ± 0.1	0.006	0.008	0.003	0.001
Cryptomonas sp. CPCC 336	1.5 ± 0.4	2.0 ± 0.5	0.3 ± 0.1	0.2 ± 0.1	0.005	0.006	0.001	0.001
Cryptomonas curvata CCAP 979/26*	36.4 ± 0.5	37.2 ± 4.7	7.6 ± 1.0	5.6 ± 1.7	0.021	0.022	0.004	0.003
Geminigera cryophila CCMP 2564	4.2 ± 0.2	7.0 ± 0.5	2.0 ± 0.1	1.1 ± 0.1	0.004	0.007	0.002	0.001
Guillardia theta CCMP 327	0.8 ± 0.1	1.2 ± 0.1	0.3 ± 0.0	0.2 ± 0.1	0.005	0.009	0.002	0.001
Hanusia phi CCMP 325	0.7 ± 0.0	0.9 ± 0.03	0.5 ± 0.0	0.3 ± 0.0	0.004	0.005	0.003	0.001
Hemiselmis andersenii CCMP 644	0.3 ± 0.0	0.6 ± 0.0	0.1 ± 0.0	0.1 ± 0.0	0.006	0.010	0.002	0.001
Hemiselmis cryptochromatica CCMP 1181	0.1 ± 0.0	0.2 ± 0.1	0.1 ± 0.0	0.1 ± 0.0	0.003	0.006	0.002	0.001
Hemiselmis pacifica CCMP 706	0.4 ± 0.0	0.5 ± 0.0	0.3 ± 0.0	0.1 ± 0.0	0.004	0.005	0.003	0.002
Hemiselmis rufescens CCMP 440	0.1 ± 0.0	0.1 ± 0.0	0.1 ± 0.0	0.1 ± 0.0	0.005	0.005	0.005	0.003
Hemiselmis tepida CCMP 443	0.1 ± 0.0	0.1 ± 0.0	0.1 ± 0.0	0.0 ± 0.0	0.003	0.006	0.002	0.001
Proteomonas sp. CCMP 2715	1.2 ± 0.0	1.9 ± 0.1	0.5 ± 0.0	0.2 ± 0.0	0.012	0.019	0.005	0.002
Proteomonas sulcata CCMP 1175	1.6 ± 0.1	3.1 ± 0.1	0.7 ± 0.0	0.4 ± 0.0	0.006	0.011	0.002	0.001
Rhinomonas reticulata CCAP 995/2	1.1 ± 0.1	1.2 ± 0.2	0.3 ± 0.0	0.2 ± 0.0	0.006	0.006	0.002	0.001
Rhodomonas abbreviata CCMP 1178	2.8 ± 0.2	4.5 ± 0.4	1.1 ± 0.0	0.8 ± 0.1	0.005	0.008	0.002	0.001
Rhodomonas atrorosea CCAP 978/6A	1.5 ± 0.1	1.3 ± 0.2	0.4 ± 0.0	0.3 ± 0.0	0.007	0.006	0.002	0.001
Rhodomonas chrysoidea NIES 701	1.9 ± 0.1	1.8 ± 0.4	0.5 ± 0.1	0.5 ± 0.0	0.007	0.007	0.002	0.002
Rhodomonas falcata NIES 702	14.0 ± 0.4	14.3 ± 0.3	3.6 ± 0.1	3.5 ± 0.1	0.034	0.034	0.009	0.008
Rhodomonas lens CCMP 739	2.3 ± 0.2	4.5 ± 0.5	0.7 ± 0.1	0.5 ± 0.1	0.008	0.016	0.002	0.001
Rhodomonas minuta CPCC 344	1.1 ± 0.0	2.0 ± 0.2	0.3 ± 0.0	0.2 ± 0.0	0.010	0.018	0.003	0.002
Rhodomonas salina CCMP 1319	1.7 ± 0.1	1.7 ± 0.1	0.5 ± 0.1	0.5 ± 0.1	0.008	0.008	0.002	0.002
Storeatula sp. CCMP 1868	15.2 ± 0.6	17.8 ± 0.2	4.0 ± 0.2	4.1 ± 0.3	0.027	0.031	0.007	0.007

(continued)

TABLE 2. (continued)

Strain	chl-a (pg·cell^{-1})	chl-c_2 (pg·cell^{-1})	Allox (pg·cell^{-1})	α-carotene (pg·cell^{-1})	chl-a (pg · μm^{-3})	chl-c_2 (pg · μm^{-3})	Allox (pg · μm^{-3})	α-carotene (pg · μm^{-3})
Unidentified sp. CCMP 1179	0.5 ± 0.1	1.1 ± 0.04	0.2 ± 0.0	0.1 ± 0.0	0.002	0.004	0.001	0.000
Unidentified sp. CCMP 2293	1.9 ± 0.1	2.7 ± 0.1	0.7 ± 0.1	0.4 ± 0.0	0.019	0.028	0.007	0.004
Unidentified sp. CCMP 3175	0.8 ± 0.0	1.2 ± 0.0	0.4 ± 0.0	0.2 ± 0.0	0.006	0.009	0.003	0.002

*Note that CCAP 979/26 was supplied to us as *Cryptomonas tetrapyrenoidosa* but that the name of this strain has been changed to *Cryptomonas curvata* (Hoef-Emden and Melkonian 2008). Values presented are means ± standard deviations of triplicate measurements. Allox = alloxanthin. Pigment per biovolume values were calculated by dividing the average pg·cell^{-1} by the average biovolume (μm^3·cell^{-1}) of each strain and therefore do not have error estimates.
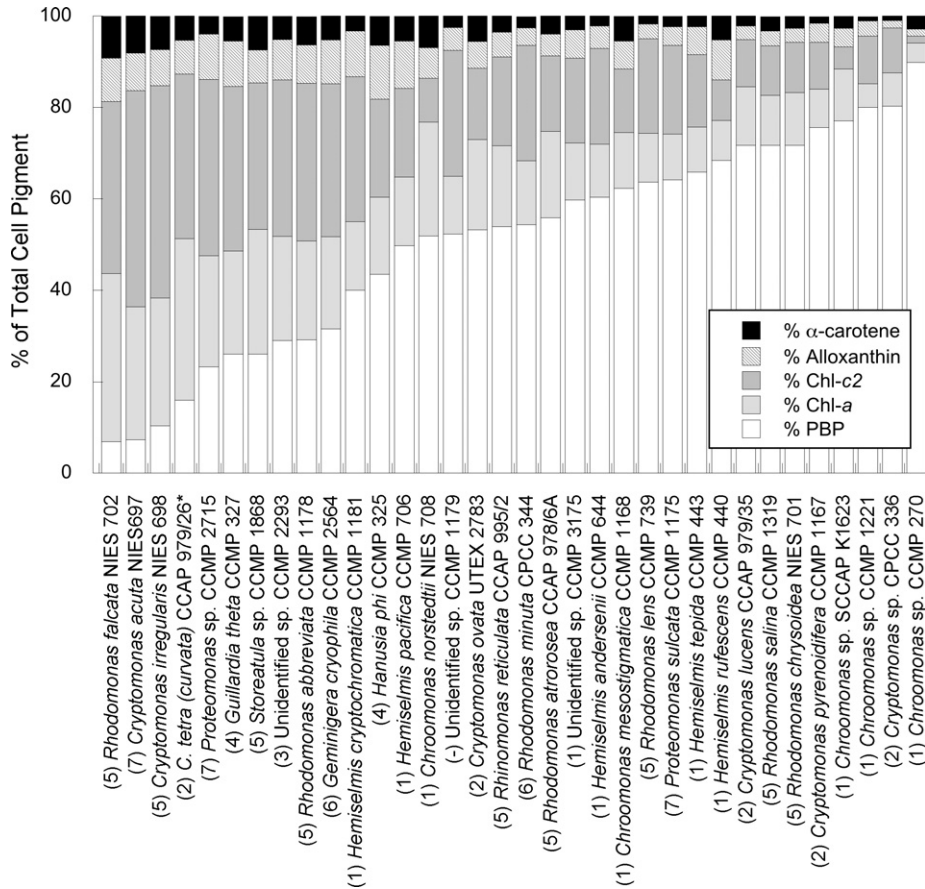

Fig. 1. Average relative concentrations (as a percentage of total cell pigment) of phycobiliprotein (PBP), chl-a, chl-c_2, alloxanthin and α-carotene for strains used in this study from lowest to highest percentage of PBP · cell^{-1}. Note that the name of CCAP 979/26 has changed from *Cryptomonas tetrapyrenoidifera* to *Cryptomonas curvata* (Hoef-Emden and Melkonian 2003) even though it is still sold as the former by the culture collection. Numbers in parentheses near the strain label show the clade number for each strain, with the exception of CCMP 1179, which did not fall into a clade (see text and Figure 2).

published cryptophyte phylogenies. Similar to previous phylogenies (Marin et al. 1998, Hoef-Emden 2008, 2018, Hoef-Emden and Archibald 2016), our data show a clade of *Hemiselmis* and *Chroomonas* strains (clade 1), a clade comprised of *Cryptomonas* strains (clade 2), a *Hanusia* and *Guillardia* dyad (clade 4) and a clade comprised of *Rhinomonas*, *Rhodomonas* and *Storeatula* strains (clade 5). Similar to recent phylogenies (Hoef-Emden 2008, Hoef-Emden and Archibald 2016), our *Hemiselmis* and *Chroomonas* clade 1 consists of three *Chroomonas* subclades and one *Hemiselmis* subclade. However, we also found several differences, which is why we did not apply previous clade numbering schemes to our
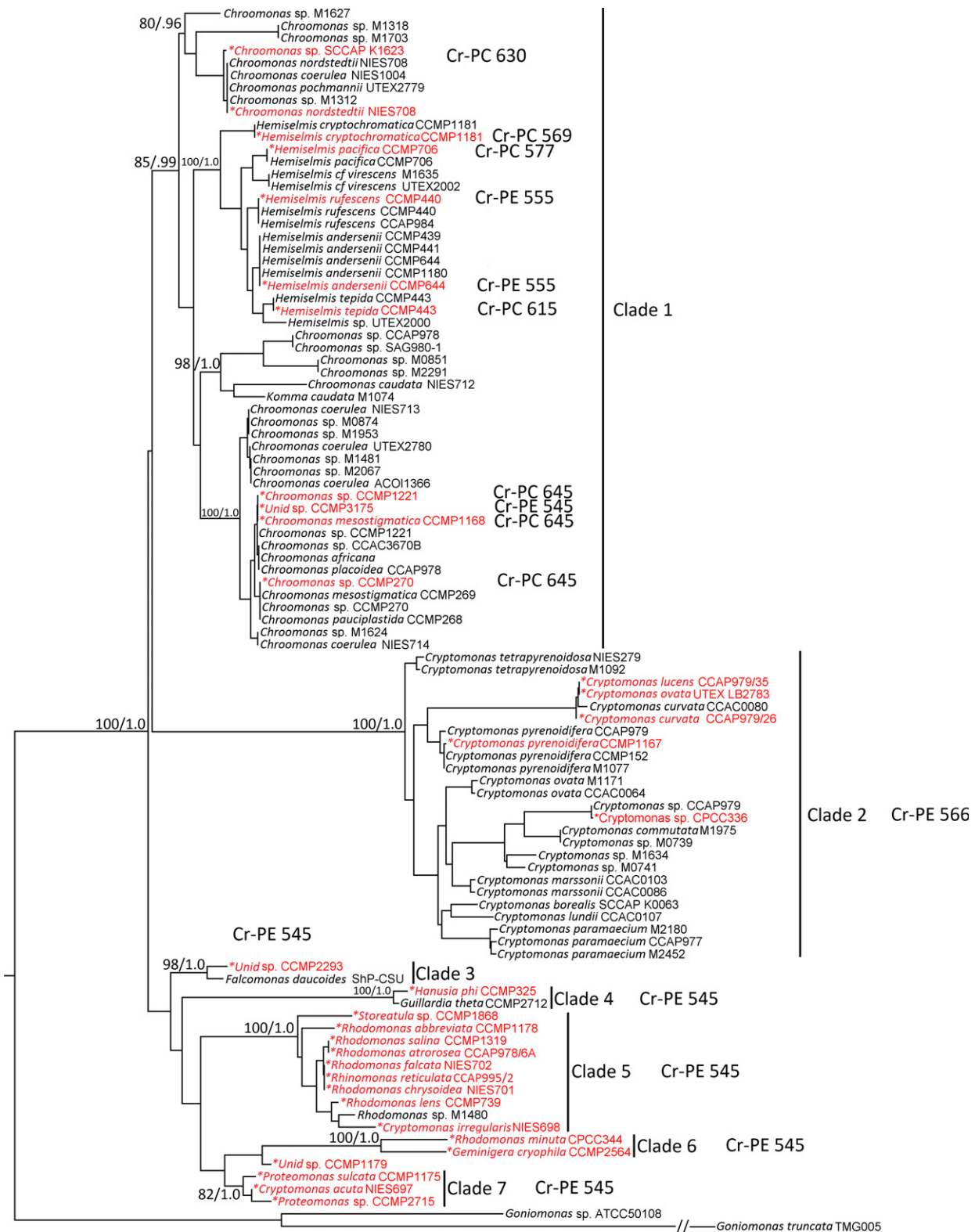
FIG. 2. Molecular phylogeny of 99 cryptophytes using nuclear SSU and partial LSU rDNA. Strains in red were sequenced and characterized by us; other sequences were downloaded from NCBI (Table S3). The topology of the phylogeny follows the maximum likelihood analysis. Two *Goniomonas* strains (*Goniomonas* sp. ATCC 50108 and *G. truncata* TMG005) were selected as outgroups. The node values are bootstrap support values from the maximum likelihood analysis and posterior probabilities from the Bayesian analysis, respectively. Note that the name of CCAP 979/26 has changed from *Cryptomonas tetrapyrenoidifera* to *Cryptomonas curvata* (Hoef-Emden and Melkonian 2003) even though it is still sold as the former by the culture collection.
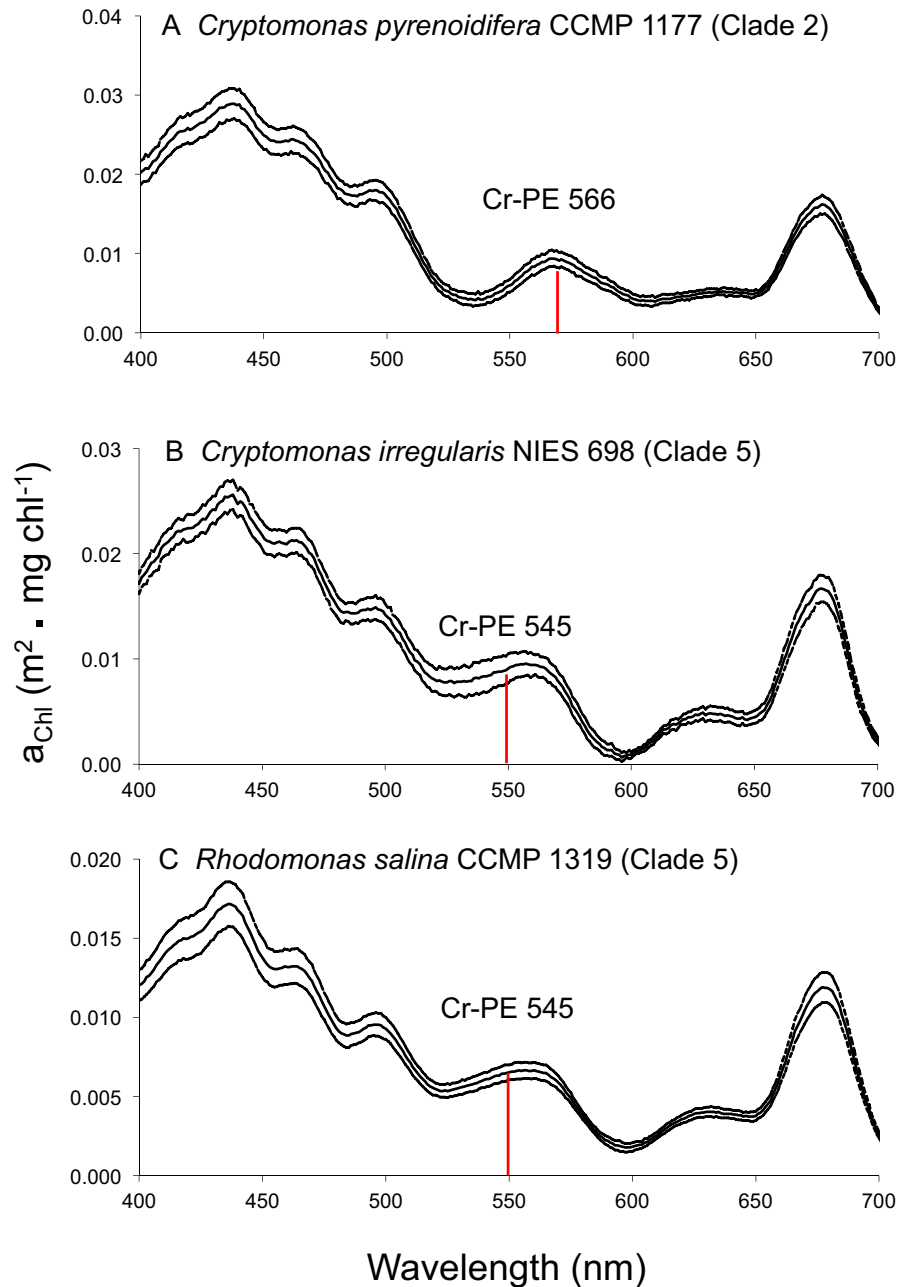
Fig. 3. Whole cell absorption spectra (normalized to total chl-*a*) for *Cryptomonas pyrenoidifera* CCMP 1177 (A), *Cryptomonas irregularis* NIES 698 (B), and *Rhodomonas salina* CCMP 1319 (C). Red lines indicate the approximate wavelength of maximum absorption by Cr-PE 566 (for *C. pyrenoidifera*) and Cr-PE 545 (for *C. irregularis* and *R. salina*).

tree. Our clade 5 (*Rhinomonas*, *Rhodomonas* and *Storeatula* strains) also contains a *Cryptomonas* strain (discussed below). Interestingly, our phylogeny resolves several previously reported (Hoef-Emden 2008, Hoef-Emden and Archibald 2016) monophyletic strains (*Proteomonas sulcata*, *Falcomonas daucoides* and unidentified strain CCMP 2293). Here, we find support for a dyad consisting of CCMP 2293 and *F. daucoides* ShP-CSU (Clade 3) and a clade consisting of a *Cryptomonas* strain and two *Proteomonas* strains (Clade

7). We found one phylogenetically isolated strain (unidentified CCMP 1179). Finally, we found a *Rhodomonas* dyad with *Geminigera cryophila*. *Geminigera* has previously been found to group with *Plagioselmis*, and *Teleaulax*, which are absent in our phylogeny (Marin et al. 1998, Hoef-Emden 2008, Hoef-Emden and Archibald 2016).

Taxonomic status of Cryptomonas irregularis. Physiologically, the *Cryptomonas. irregularis* NIES 698 strain within our clade 5 is a marine strain, appears reddish
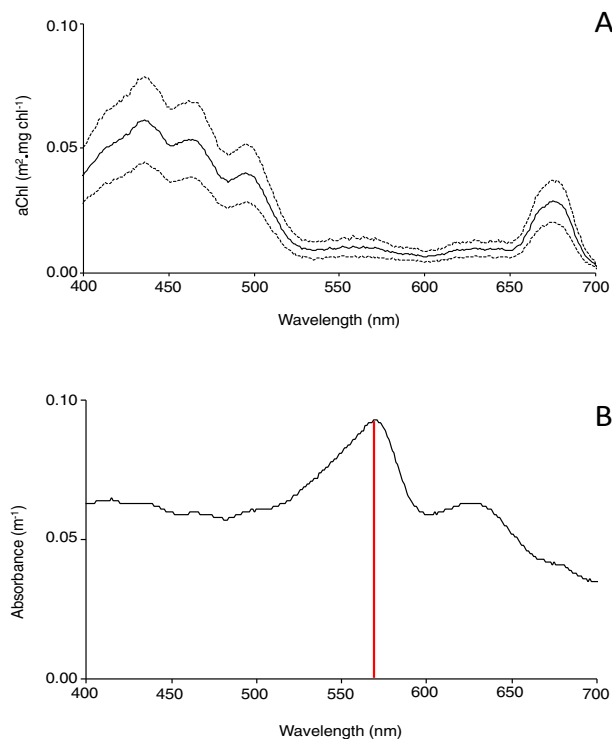
Hemiselmis cryptochromatica CCMP 1181

FIG. 4. Optical properties of *Hemiselmis cryptochromatica* CCMP 1181. (A) The whole cell absorption spectrum, normalized to chlorophyll-*a* concentration. The solid line is the average of triplicate samples and the dotted line indicates standard deviation. (B) A representative absorption spectrum for phycobiliproteins extracted from *H. cryptochromatica* CCMP 1181, with the absorption peak (red line) at 569 nm.

in color, and contains Cr-PE 545. These are all characteristics of *Rhodomonas*, *Rhinomonas*, and *Storeatula*. In contrast, the *Cryptomonas* of Clade 2 are freshwater strains, appear gray/brown, and contain Cr-PE 566.

Since several phenotypic characteristics (e.g., PBP absorption peak, whole cell absorption spectra, and pigment concentrations) of *Cryptomonas irregularis* NIES 698 were unusual for a *Cryptomonas* strain, we examined the published cellular ultrastructural data and the placement of this strain within our phylogeny to clarify genus classification. A previous study compared the cellular ultrastructure of several *Rhodomonas* strains to the ultrastructure of a strain of *C. irregularis* (Erata and Chihara 1989). That study concluded that their strain of *C. irregularis* should be reclassified as *Rhodomonas irregularis*. Our molecular and phenotypic data corroborate that conclusion.

Revised PBP diversity within Hemiselmis. The *Hemiselmis* group in clade 1 contains the greatest diversity of PBP pigments among the cryptophytes (Cr-PE 555, Cr-PC 569, 577, and 615). Prior work indicates that *H. cryptochromatica* (CCMP 1181) is the only known *Hemiselmis* strain to contain an additional PBP, Cr-PC 630 (Hoef-Emden 2008, Lane and Archibald 2008, Hoef-Emden and Archibald 2016), which otherwise is found only in *Chroomonas*. In contrast, our data indicate that *H. cryptochromatica* contains Cr-PC 569 (Fig. 4). The dual absorption peaks of the PBP extracted from *H. cryptochromatica* CCMP 1181 (Fig. 4B) match the major 569 nm and minor 630 nm absorption peaks previously described for another cryptophyte that contains Cr-PC 569 (*F. daucoides*; Hill and Rowan 1989) and do not match our *Chroomonas* strains that have Cr-PC 630. We note that the relatively low PBP concentration ($0.27 \text{ pg} \cdot \text{cell}^{-1}$) of *H. cryptochromatica* made absorption spectra challenging to acquire, and required us to filter a higher than usual volume of *H. cryptochromatica* CCMP 1181 for analysis. However, the acquired spectra show distinct peaks, and we conclude that *H. cryptochromatica* CCMP 1181 contains Cr-PC 569 and not Cr-PC 630.

The identity of unidentified strain CCMP 2293. Previous studies have indicated that the strain CCMP 2293 belongs to the genus *Falcomonas* (Potvin and Lovejoy 2009, Terrado et al. 2011), although the strain is still formally an unidentified strain. Our CCMP 2293 is a reddish–brown strain that we believe contains Cr-PE 545 (Fig. S7 in the Supporting Information). An additional strain belonging to *Falcomonas* is blue-green in appearance and contains Cr-PC 569 (Hill 1991, Clay and Kugrens 1999), while Raho et al. (2014) report that CCMP 2045 is 84.6% similar in sequence to known *Falcomonas* strains. Also, our CCMP 2293 is an Arctic isolate grown at 4°C, while *F. daucoides* is reported to be grown at 18°C (Clay and Kugrens 1999). So, if CCMP 2293 does belong to the genus *Falcomonas*, this indicates that the genus is more diverse than previously recognized, and that it contains at least two different PBP types.

Discovery of a red "Chroomonas". Strains of *Chroomonas* are known to contain either Cr-PC 630 or 645, which causes these cells to appear green in color (Hoef-Emden and Archibald 2016). Our phylogeny indicates that unidentified strain CCMP 3175 resides within Clade 1, but our phenotypic data show it to be red in color and to contain Cr-PE 545 (Fig. 5). A new revision of the *Chroomonas* genus (Hoef-Emden (2018) based on DNA sequencing and ultrastructure shows that there are at least two sub-clades within the original *Chroomonas* clade that may not belong to *Chroomonas*. The cell lengths of CCMP 3175 indicate that it may fall into one of these subclades. However, even if future taxonomic revision divides the genus *Chroomonas* into three or more genera, the division is unlikely to reflect differences in PBPs. This is because CCMP 3175, although it has Cr-PE 545, clearly fell into a clade of three strains where the others all contain Cr-PC 645. Continued physiological and genetic analysis, plus evaluation of cellular ultrastructure, will be necessary to resolve fully the taxonomy of *Chroomonas* and closely related genera.
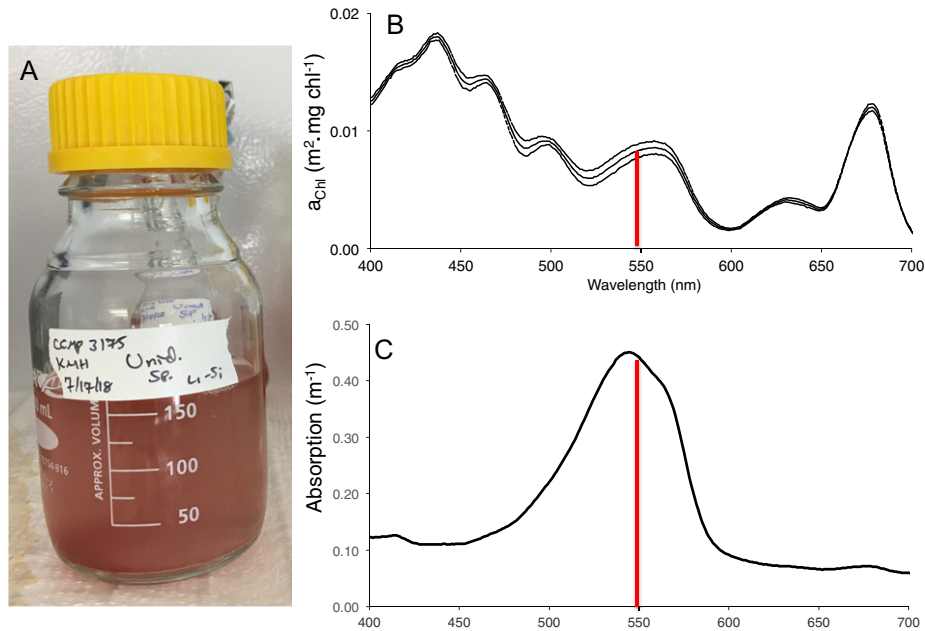
FIG. 5. Appearance and absorption properties of unidentified strain CCMP 3175. (A) Cells in culture. (B) The whole cell absorption spectrum (mean ± SD of triplicate measurements), normalized to chl-a. (C) A typical absorption spectrum for phycobiliproteins extracted from CCMP 3175, with a peak near 545 nm.

Phenotype-based predictions of molecular phylogeny. Results of our discriminant analysis showed that PBP · cell^{-1}, maximum absorption wavelength of that PBP, and habitat were fairly good, but not perfect, predictors of clade membership. The visual appearance of a strain is not necessarily a good indicator of either genus or PBP type (see also Hoef-Emden and Archibald 2016). As an example, *Hemiselmis phi* CCMP 325 and *Hemiselmis cryptochromatica* CCMP 1181 look similar in appearance and have similar whole cell absorption spectra (data not shown) but different PBP types (Cr-PE 545 vs. Cr-PE 569, respectively). Strain color may also vary with nutrient availability, particularly with nitrogen scarcity, which decreases the rate of PBP synthesis or may even result in breakdown of cellular PBP to release nitrogen (Lewitus and Caron 1990, Guevara et al. 2016). Researchers now prefer to combine light and electron microscope observations of cellular ultrastructure with molecular phylogenetic analyses to identify and classify cryptophytes (e.g., Hoef-Emden 2007, Lane and Archibald 2008).

It is intriguing to note that none of the other phenotypic traits (chl-a, chl-c_2, alloxanthin, or α-carotene concentration · cell^{-1} or · μm^{-3}) were good predictors of clade classification. This result suggests that pigments other than the PBPs played a limited role in the evolutionary divergence of cryptophyte genera. Our pigment analysis also shows that cellular concentrations of PBPs are generally inversely proportional to the concentration of chlorophylls ($a + c_2$), which suggests a trade-off in investments in these different pigments. These apparent trade-offs span the range of relative concentrations of PBPs, with no clear phylogenetic pattern.

CONCLUSIONS

We have provided the first phylogenetically broad comparison of key traits involved in light capture within the Cryptophyta, a eukaryotic phylum known for its diversity in pigmentation and color. The combination of phenotypic data with phylogenetic information allowed us to lend support to previous studies that propose genus-level classification for unidentified strain CCMP 2293 into *Falcomonas* and a revised genus of a second (*Cryptomonas irregularis* NIES 698 into *Rhodomonas*). Further, we add to the PBP diversity within the *Hemiselmis* clade through providing evidence for the inclusion of *Hemiselmis cryptochromatica* CCMP 1181 that contains Cr-PC 569. Finally, we provide evidence that, despite it being red in appearance and containing Cr-PE 545, CCMP 3175 should be included with Clade 1 "*Chroomonas*" species, but that its exact genus classification is currently under revision.

CONFLICTS OF INTEREST

The authors declare no conflicts of interest.

Andersen, R. A. 2005. *Algal Culturing Techniques*. Elsevier Academic Press, San Diego, CA 578 pp.

Archibald, J. M. & Keeling, P. J. 2002. Recycled plastids: a "green movement" in eukaryotic evolution. *Trends Genet.* 18:577–84.

Bhattacharya, D., Yoon, H. S. & Hackett, J. D. 2004. Photosynthetic eukaryotes unite: endosymbiosis connects the dots. *BioEssays* 26:50–60.

Clay, B. L. & Kugrens, P. 1999. Characterization of *Hemiselmis amylosa* sp. nov. and phylogenetic placement of the blue-green cryptomonads *H. amylosa* and *Falcomonas daucoides*. *Protist* 150:297–310.

Erata, M. & Chihara, M. 1989. Re-examination of *Pyrenomonas* and *Rhodomonas* (class Cryptophyceae) through ultrastructural survey of red pigmented cryptomonads. *Bot. Mag. Shokubutsu-gaku-zasshi.* 102:429.

Gantt, E. 1979. Phycobilins of the Cryptophyceae. In Levandowsky, M. & Hutner, S.H. *Biochemistry and Physiology of the Protozoa, Vol. 1*, 2nd. ed., Elsevier Academic Press, San Diego, California, pp. 121–37.

Gelman, A. & Rubin, D. B. 1992. Inference from iterative simulation using multiple sequences. *Stat. Sci.* 7:457–511.

Glazer, A. N. & Wedemayer, G. J. 1995. Cryptomonad biliproteins —an evolutionary perspective. *Photosynth. Res.* 46:93–105.

Gould, S. B., Fan, E., Hempel, F., Maier, U. G. & Klösgen, R. B. 2007. Translocation of a phycoerythrin α subunit across five biological membranes. *J. Biol. Chem.* 282:30295–302.

Gould, S. B., Waller, R. F. & Mcfadden, G. I. 2008. Plastid evolution. *Annu. Rev. Plant Biol.* 59:491–517.

Guevara, M., Arredondo-Vega, B. O., Palacios, Y., Saéz, K. & Gómez, P. I. 2016. Comparison of growth and biochemical parameters of two strains of *Rhodomonas salina* (Cryptophyceae) cultivated under different combinations of irradiance, temperature, and nutrients. *J. Appl. Phycol.* 28:2651–60.

Guillard, R. R. L. & Sieracki, M. S. 2005. Counting cells in cultures with the light microscope. *In* Andersen, R. A. [Ed.] *Algal Culturing Techniques*. Elsevier Academic Press, San Diego, California, pp. 239–52.

Hall, T. A. 1999. BioEdit: a user-friendly biological sequence alignment editor and analysis program for Windows 95/98/NT. *Nucl. Acids Symp. Ser.* 41:95–8.

Hill, D. R. A. 1991. *Chroomonas* and other blue-green cryptomonads. *J. Phycol.* 27:133–45.

Hill, D. R. A. & Rowan, K. S. 1989. The biliproteins of the cryptophyceae. *Phycologia* 28:455–63.

Hillebrand, H., Dürselen, C. D., Kirschtel, D., Pollingher, U. & Zohary, T. 1999. Biovolume calculation for pelagic and benthic microalgae. *J. Phycol.* 35:403–24.

Hoef-Emden, K. 2007. Revision of the genus Cryptomonas II: incongruences between the classical morphospecies concept and molecular phylogeny in smaller pyrenoid-less cells. *Phycologia* 46:402–28.

Hoef-Emden, K. 2008. Molecular phylogeny of phycocyanin-containing cryptophytes: evolution of biliproteins and geographical distribution. *J. Phycol.* 44:985–93.

Hoef-Emden, K. 2018. Revision of the genus *Chroomonas* Hansgirg: the benefits of DNA-containing specimens. *Protist* 169:662–81.

Hoef-Emden, K. & Archibald, J. M. 2016. Cryptophyta (Cryptomonads). *In* Archibald, J. M. [Ed.] *Handbook of the Protists.* Springer International Publishing AG, Cham, Switzerland, pp. 1–41.

Hoef-Emden, K. & Melkonian, M. 2003. Revision of the Genus *Cryptomonas* (Cryptophyceae): a combination of molecular into a long-hidden dimorphism. *Protist* 154:371–409.

Hoef-Emden, K. & Melkonian, M. 2008. Corrigendum to revision of the genus *Cryptomonas* (Cryptophyceae): a combination of molecular phylogeny and morphology provides insights into a long-hidden dimorphism. *Protist* 159:507.

Kamiya, A. & Miyachi, S. 1984. Effects of light quality on formation of 5-aminolevulinic acid, phycoerythrin and chlorophyll in *Cryptomonas* sp. cells collected from the subsurface chlorophyll layer. *Plant Cell Physiol.* 25:831–9.

Klaveness, D. 1988. Biology and ecology of the Cryptophyceae: status and challenges. *Biol. Oceanogr.* 6:257–70.

Lane, C. E. & Archibald, J. M. 2008. New marine members of the genus *Hemiselmis* (Cryptomondales, Cryptophyceae). *J. Phycol.* 450:439–50.

Lanfear, R., Frandsen, P. B., Wright, A. M., Senfeld, T. & Calcott, B. 2016. PartitionFinder 2: new methods for selecting partitioned models of evolution for molecular and morphological phylogenetic analyses. *Mol. Biol. Evol.* 34:msw260.

Larkin, M. A., Blackshields, G., Brown, N. P., Chenna, R., Mcgettigan, P. A., McWilliam, H., Valentin, F. et al. 2007. Clustal W and Clustal X version 2.0. *Bioinformatics* 23:2947–8.

Lawrenz, E., Fedewa, E. J. & Richardson, T. L. 2011. Extraction protocols for the quantification of phycobilins in aqueous phytoplankton extracts. *J. Appl. Phycol.* 23:865–71.

Lewitus, A. J. & Caron, D. A. 1990. Relative effects of nitrogen or phosphorus depletion and light intensity on the pigmentation, chemical composition, and volume of *Pyremonas salina* (Cryptophyceae). *Mar. Ecol. Prog. Ser.* 61:171–81.

Lund, J. W. G., Kipling, C. & Le Cren, E. D. 1958. The inverted microscope method of estimating algal numbers and the statistical basis of estimations by counting. *Hydrobiologia* 11:143–70.

MacColl, R., Habig, W. & Berns, D. S. 1973. Characterization of phycocyanin from Chroomonas species. *J. Biol. Chem.* 248:7080–86.

MacColl, R., Berns, D. S. & Gibbons, O. 1976. Characterization of cryptomonad phycoerythrin and phycocyanin. *Arch. Biochem. Biophys.* 177:265–75.

Marin, B., Klingberg, M. & Melkonian, M. 1998. Phylogenetic relationships among the Cryptophyta: analyses of nuclear-encoded SSU rRNA sequences support the monophyly of extant plastid-containing lineages. *Protist* 149:265–76.

Morel, A. 1978. Available, usable, and stored radiant energy in relation to marine photosynthesis. *Deep Sea Res.* 25:673–88.

Nicklisch, A. & Steinberg, C. E. W. 2009. RNA/protein and RNA/DNA ratios determined by flow cytometry and their relationship to growth limitation of selected planktonic algae in culture. *Eur. J. Phycol.* 44:297–308.

Overkamp, K. E., Langklotz, S., Aras, M., Helling, S., Marcus, K., Bandow, J. E., Hoef-Emden, K. & Frankenberg-Dinkel, N. 2014a. Chromophore composition of the phycobiliprotein Cr-PC577 from the cryptophyte Hemiselmis pacifica. *Photosyn. Res.* 122:293–304.

Overkamp, K. E., Gasper, R., Kock, K., Herrmann, C., Hofmann, E. & Frankenberg-Dinkel, N. 2014b. Insights into the biosynthesis and assembly of cryptophycean phycobiliproteins. *J. Biol. Chem.* 289:26691–707.

Pattengale, N., Alipour, M., Bininda-Emonds, O., Moret, B. & Stamatakis, A. 2009. How many bootstrap replicates are necessary? *J. Comput. Biol.* 5541:184–200.

Pinckney, J. L., Millie, D. F., Howe, K. E., Paerl, H. W. & Hurley, J. P. 1996. Flow scintillation counting of ^{14}C-labeled microalgal photosynthetic pigments. *J. Plankton Res.* 18:1867–80.

Potvin, M. & Lovejoy, C. 2009. PCR-based diversity estimates of artificial and environmental 18S rRNA gene libraries. *J. Eukaryot. Microbiol.* 56:174–81.

Raho, N., Jaén, D., Mamán, L., Rial, P. & Marín, I. 2014. psbA based molecular analysis of cross-feeding experiments suggests that *Dinophysis acuta* does not harbour permanent plastids. *Harmful Algae* 35:20–8.

Rice, P., Longden, I. & Bleasby, A. 2000. EMBOSS: the European Molecular Biology Open Software Suite. *Trends Genet.* 16:276–7.

Roesler, C. S. 1998. Theoretical and experimental approaches to improve the accuracy of particulate absorption coefficients derived from the quantitative filter technique. *Limnol. Oceanogr.* 43:1649–60.

Ronquist, F., Teslenko, M., Van Der Mark, P., Ayres, D. L., Darling, A., Höhna, S., Larget, B., Liu, L., Suchard, M. A. & Huelsenbeck, J. P. 2012. Mrbayes 3.2: efficient Bayesian phylogenetic inference and model choice across a large model space. *Syst. Biol.* 61:539–42.

Shibata, B. Y. K. 1958. Spectrophotometry of intact biological materials. *J. Biochem.* 45:599–624.

Stamatakis, A. 2014. RAxML version 8: a tool for phylogenetic analysis and post-analysis of large phylogenies. *Bioinformatics* 30:1312–3.

Stucky, B. J. 2012. SeqTrace: a graphical tool for rapidly processing DNA sequencing chromatograms. *J. Biomol. Tech.* 23:90–3.

Terrado, R., Medrinal, E., Dasilva, C., Thaler, M., Vincent, W. F. & Lovejoy, C. 2011. Protist community composition during spring in an Arctic flaw lead polynya. *Polar Biol.* 34:1901–14.

Vesk, M. & Jeffrey, S. W. 1977. Effect of blue-green light on photosynthetic pigments and chloroplast structure in unicellular marine algae from six classes. *J. Phycol.* 13:280–8.

Supporting Information

Additional Supporting Information may be found in the online version of this article at the publisher's web site:

Figure S1. Cryptophyte cultures showing range in coloration and phycobiliprotein type, from left to right: *Rhodomonas salina* CCMP 1319, *Hemiselmis andersenii* CCMP 644, *Cryptomonas ovata* UTEX 2783, *Hemiselmis cryptochromatica* CCMP 1181, *Hemiselmis pacifica* CCMP 706, *Hemiselmis tepida* CCMP 443, *Chroomonas* sp. SCCAP K1623, and *Chroomonas mesostigmatica* CCMP 1168.

Figure S2. Whole cell absorption spectra, normalized to chlorophyll-*a* concentration, for representative strains shown in Figure S1 (A–H), each having a different type of phycobiliprotein as indicated. The solid vertical line in each panel represents the peak of maximum absorption for each PBP. Presented are means (solid lines) ± standard deviations (dashed lines; n = 3).

Figure S3. Same as Figure 2, but more easily scalable.

Figure S4. Whole cell absorption spectra, normalized to chlorophyll-*a* concentration, for *Cryptomonas acuta* NIES 697 (A), *Cryptomonas irregularis* NIES 698 (B), and *Rhodomonas salina* CCMP 1319 (C). Red lines indicate the approximate wavelength of maximum absorption of the phycobiliprotein pigment Cr-PE 545 found in each strain.

Figure S5. Absorption spectra for extracted phycobiliprotein pigments from cryptophyte strains that were classified into Clade 1. The three *Chroomonas* strains contain Cr-PC 645 but the unidentified species CCMP 3175 instead contains Cr-PE 545.

Figure S6. Absorption spectra for phycobiliproteins extracted from *Hemiselmis* strains classified into Clade 1.

Figure S7. Appearance and absorption properties of unidentified strain CCMP 2293. (A) Cells in culture. (B) Whole cell absorption spectrum (mean ± SD of triplicate measurements), normalized to chl-*a*. (C) A typical absorption spectrum for phycobiliproteins extracted from CCMP 2293, with a peak near 545 nm.

Table S1. Culture conditions and sources for the cryptophyte strains used in this study. Source collections and their abbreviations: Culture Collection of Algae and Protozoa (CCAP); National Center for Marine Algae and Microbiota (NCMA, formerly CCMP); The Culture Collection of Algae at the University of Texas at Austin (UTEX); Microbial Culture Collection at the National Institute for Environmental Studies (NIES); Canadian Phycological Culture Center (CPCC); Scandinavian Culture Collection of Algae and Protozoa (SCCAP). *Note that CCAP 979/26 was supplied to us as *Cryptomonas tetrapyrenoidosa* but that the name of this strain has been changed to *Cryptomonas curvata* (Hoef-Emden and Melkonian 2008). Recipes for most media can be found in the appendices of Andersen (2005). Org = organic supplement.

Table S2. List of PCR and sequencing primers.

Table S3. Accession numbers for cryptophyte strains in our phylogeny.

Table S4. Results of step-wise discriminant analyses to predict clade classification from phenotypic and habitat characteristics of 33 strains of cryptophytes. Variables included in the analysis: habitat (freshwater, marine or estuarine), cell biovolume (μm^3), wavelength of maximum absorption by phycobiliprotein pigments (PBP peak abs), PBP per cell, PBP $\cdot \mu m^{-3}$, chl-*a* per cell, chl-$a \cdot \mu m^{-3}$, chl-c_2 per cell, chl-$c_2 \cdot \mu m^{-3}$, alloxanthin per cell, alloxanthin $\cdot \mu m^{-3}$, α-carotene per cell and α-carotene $\cdot \mu m^{-3}$. Three variables (in bold) explained 77.8% of the variance and correctly classified 70.6% of the original grouped cases.